Politecnico di Torino

Porto Institutional Repository

[Article] Magnetic dipolar coupling and collective effects for binary information codification in cost-effective logic devices

(Article begins on next page)
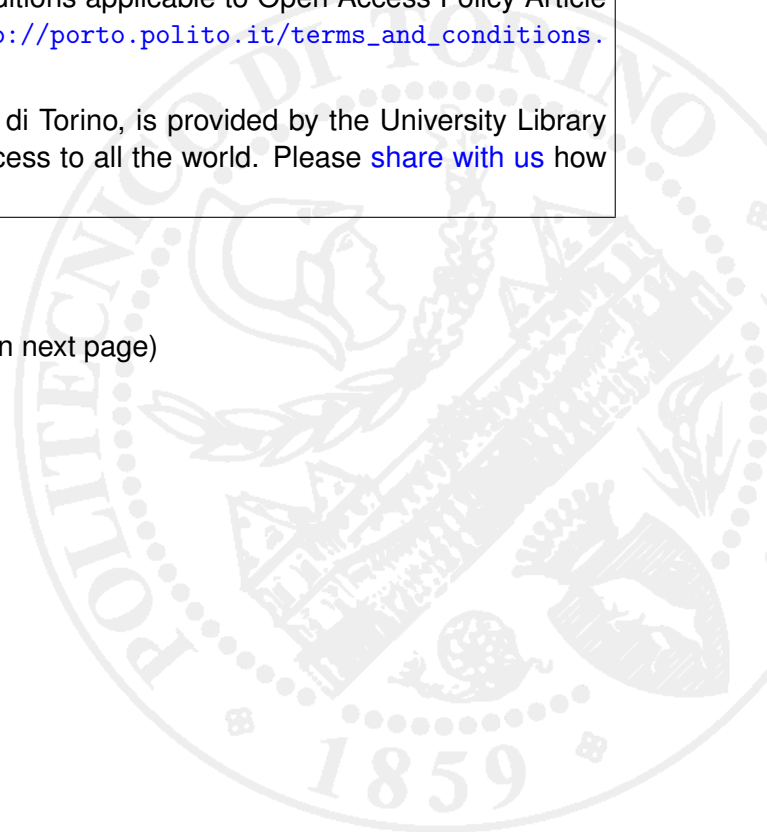
Magnetic dipolar coupling and collective effects for binary information codification

Alessandro Chiolerio[1]*, Paolo Allia[2] and Mariagrazia Graziano[3]

[1]Physics Department, Politecnico di Torino, Corso Duca degli Abruzzi 24, IT-10129, Torino - Italy
* alessandro.chiolerio@polito.it; Tel. +39 011 5647381; Fax + 39 011 5647399.
[2]Materials Science and Chemical Engineering Department, Politecnico di Torino, Corso Duca degli Abruzzi 24, IT-10129, Torino - Italy
[3]Electronic Department, Politecnico di Torino, Corso Duca degli Abruzzi 24, IT-10129, Torino - Italy

Physical limitations foreshadow the eventual end to traditional Complementary Metal Oxide Semiconductor (CMOS) scaling. Therefore, interest has turned to various materials and technologies aimed to succeed to traditional CMOS. Magnetic Quantum dot Cellular Automata (MQCA) are one of these technologies. Working MQCA arrays require very complex techniques and an excellent control on the geometry of the nanomagnets and on the quality of the magnetic thin film, thus limiting the possibility for MQCA of representing a definite solution to cost-effective, high density and low power consumption device demand. Counter-intuitively, moving towards bigger sizes and lighter technologies it is still possible to develop multi-state logic devices, as we demonstrated. We realized cobalt micrometric MQCA arrays by means of Electron Beam Lithography, exploiting cost-effective processes such as lift-off and RF sputtering that usually are avoided due to their low control on array geometry and film roughness. Information relative to the magnetic configuration of MQCA elements including their eventual magnetic interactions was obtained from Magnetic Force Microscope (MFM) images, enhanced by means of a numerical procedure and presented in differential maps. We report the existence of bi-stable magnetic patterns, as detected by MFM while sampling the z-component of magnetic induction field, arising from dipolar inter-element magnetostatic coupling, able to store and propagate binary information. This is achieved despite the array quality and element magnetic state, which are low and multi-domain,

respectively. We discuss in detail shape, inter-element spacing and dot profile effects on the magnetic coupling. Numerical Finite Element Method (FEM) simulations show a possible microspin arrangement producing such magnetostatic coupling.

1. Introduction

The MQCA concept is a version of the field coupled Quantum Cellular Automata (QCA) architecture that was first proposed by Lent [1]. The original idea was introduced for a quantum dot system where electrons tunnel between the quantum dots under the influence of repelling Coulomb forces. An elementary building block contains four quantum dots in a square arrangement, having one dot in each corner. With two electrons in the four-dot cell, two stable states are defined by the configuration of the electrons as they occupy the corners of the squares along the diagonals. Electron tunneling occurs only inside the cells, and the neighboring boxes are coupled by long-range electrostatic fields. This architecture can propagate and process binary information when a feasible clocking method is applied [2].

From a more general point of view, the field-coupled QCA architecture is a signal processing system built from simple, identical, bi-stable units that are locally connected to each other solely by electromagnetic forces; consequently, the signal processing function is defined by the relative position of the building blocks and their physical interactions.

The first experimental demonstration of a working electronic QCA cell was published in 1997, the logic gate in 1999 and the shift register in 2003, by the group of the University of Notre Dame [3-5]. They proposed to realize the Magnetic QCA concept using ferromagnetic dots and magnetic field coupling. The basic geometry exploits the anti-parallel coupling between two identical elements. As an advantage compared to the above mentioned electrostatic devices, logic gates featuring single-domain magnets in the size scale of 100 nm are expected to operate at room temperature, because of the

relatively high coupling energy [6]. However, very expensive equipment and an excellent control on the geometries and materials are required to operate on those scales.

In this work we report a stable and robust magnetostatic inter-element interaction by means of dipolar coupling using room-temperature equipment and featuring RF sputtered Co elements, with micrometric major axis and micrometric spacing. Our results, substantiated by means of enhanced MFM differential imaging, show that a bi-stable magnetic field distribution develops in the volume containing the patterned elements even though the intra-element magnetic configuration is not that of a single state domain. This finding opens the route to a multi-domain implementation of the MQCA concept.

2. Materials and Methods

MQCA patterns were prepared by means of Electron Beam Lithography (EBL). We used Si (100) substrates, with a thermally evaporated bi-layer of Ti/Cu, 5 and 150-nm-thick. Substrates were spin-coated with two PMMA layers featuring different densities in order to optimize the following lift-off step: a low Molecular Weight (MW) PMMA solution was spin-coated and heated at 160 °C for 10 min on a hotplate, then high MW PMMA was spin-coated and heated at the same conditions [7]. Field Effect Secondary Electron Microscope (FESEM) and Atomic Force Microscope (AFM) analysis showed no pitting of the evaporated substrates. The antidot pattern consisted in a rectangular lattice of elliptical cylinders separated by a varying distance, resulting in non-interacting elements, weakly interacting elements and interacting elements showing collective behavior. Spin-coated samples were exposed to an electron beam whose current was 10-12 pA. Removal was done with MIBK:IPA (Methyl-Isobutyl-Ketone:Isopropyl-Alcohol) developer. A continuous Co film was deposited by RF magnetron sputtering at 10 mTorr in Ar (base pressure 6×10^{-8} Torr) and RF power of 75 W at room temperature. Co resulted to be polycrystalline and composed by a mixture of fcc and hcp phases with nanometric grains, as determined by XRD and XPS [8], showing a substantial refinement of grains with respect to thermally evaporated magnetic thin films previously studied [9,10]. Film thickness was 55 nm as determined by AFM analysis. Finally, removal of unexposed PMMA was done with a solution of N-Methyl Pyrrolidone, heated at 120 °C to increase its removal power.

AFM/MFM measurements were performed for obtaining topographical and magnetic tip/sample interaction matrices: the MQCA were investigated by Lift Mode MFM (DI NanoScope III) using high coercivity commercial tips (NSC, Co-Cr coated). Magnetic force gradients were measured in the frequency modulation mode. Lift height was set to 100 nm. Frames were acquired over the same sample area submitted to a static magnetic field aligned with the elements' major axis, in the range -100 / +100 Oe, applied in the array plane by two Helmholtz coils. Sample scans were taken in air at room temperature. The samples were demagnetized before each MFM measurement by using an alternating, out of plane magnetic field of reducing amplitude in order to start each measurement run with a repeatable reference configuration.

An enhancement procedure was performed, with the aim of eliminating or reducing possible artifacts and interactions between MFM tip and sample [11]. Figure 1 shows the typical flowchart of such a procedure: both the AFM and MFM image data sets, acquired at different magnetic fields, are subjected to preconditioning and conversion to an algebraically open format; then image registration (the treatment that allows to perfectly match and superimpose different pictures of the same scene, recovering any accidental sample shift or scanner instability) is performed based on the sample morphology (AFM) and adapted to magnetic contrast (MFM). An overall sum of MFM frames is then computed, the Systematic Error Map (SEM), containing information which is common to all the acquired frames. The SEM is subtracted from each frame, which now is noise-free and can be compared to the others. A full differential approach, in which the magnetic configuration recorded at negative field (negative remanence) is algebraically subtracted from that recorded at positive field (positive remanence), avoids the erroneous detection of tip magnetization reversals, as we already demonstrated [12].

Figure 1. Differential magnetic enhancement procedure flowchart. The field value is expressed in Oe; the sign at apex above zero identifies the last saturation reached by the sample, either negative ("0^-") or positive ("0^+").

3. Results

MQCA arrays of elliptical Co cylinders arranged in a rectangular lattice were characterized by means of FESEM analysis to evaluate the surface morphology and the

grain size. The sample shown in Figure 2 consists of a square array of non-interacting elements (geometry A) where the inter-element distance along the major axis is 11 µm, while along the minor axis is 4.5 µm. The single element aspect ratio (major over minor axis) was set to 2; the reason for this choice was to improve magnetization switching, by increasing the shape anisotropy and stabilizing one configuration in particular, the one with magnetization fully aligned with the major axis [13]. Referring to Figure 2, the bright contour of each element is due to the deposition technique, which produces sharp exposed edges after lift-off and a concave shape, resulting in a greater secondary electron emission when imaged at FESEM. The typical tolerance of our process is 2%, both on the size of each element (both major and minor axis) and on the inter-element distance (both directions), while on the mean element thickness the uniformity is 5%. We observed that roughly 50% of the contour is perfectly matched by a regular osculating ellipse while the remainder presents a mismatch typical of the lift-off procedure, consisting of a fringe whose radial extension ranges from 10 to 20 nm (worst case, as already declared, resulting in a 2% of error). The mean grain size of each Co element is below 50 nm (see [8]), while the mean grain size of the metalized substrate is around 20 nm. We point out that deviations from ideal geometry (due to lift-off), ideal section profile of each pillar (due to sputtering) and ideal roughness of the magnetic thin film (due to sputtering and substrate roughness) are a fundamental premise of this work. In fact we will conclude that these imprecise but fast and cost-effective techniques are suitable for the implementation of a binary magnetostatic logic.

Other samples were produced gradually reducing the inter-element spacing along both the minor and major axis direction as well as increasing the aspect ratio over 4, in order to increase the shape anisotropy. Two geometries, referred to as B and C, featuring respectively weakly interacting and strongly interacting elements were prepared. Geometry B is such that each element is elliptical, roughly 1650 nm in the major axis, featuring an aspect ratio of 4.25, having a spacing of 2.2 µm along the major axis and 1.5 µm along the minor one. Geometry C is such that the same arrangement as in geometry B is produced between elements featuring an aspect ratio of 4.5, obtained by reducing their minor axis.

Figure 2. FESEM image of a non-interacting Co elliptical elements, sample A. On the left column the major axis lengths are indicated, while on the right column the minor ones are.

By applying a magnetic field, we could observe by MFM the collective behavior of the patterned samples, ranging from a weaker interaction that produces faint magnetic induction field in the volume surrounding the MQCA elements to stronger interactions influencing the z-component of magnetic induction field in the space between elements. The AFM profile shown in Figure 3a is related to sample C; the gray scale has been stretched to better show the low thickness variations in correspondence of the top of each pillar, hence the substrate appears black and dust particles appear white. Dust particles are identified as bright spots without magnetic contrast in the corresponding MFM image, shown in Figure 3b: one is clearly visible close to the right edge. Some stiff material (Co) is accumulated in correspondence of the ellipse edge; this magnetic material is identified since in the corresponding MFM image a signal appears. Figure 3b represents a registered frame acquired with an external field of -100 Oe directed along the major axis. It is not easy to read both the inter-element magnetic field distribution and the intra-element magnetization configuration. For this reason a double differential computation was performed: the algebraic sum of all the acquired frames (0, -100, 0, +100, 0 Oe represents a full cycle) was subtracted from each one [14]. The results are presented in Figure 3c and d, relative to a single element magnetic field distribution (sample C again) when submitted to -100 and +100 Oe respectively. It is clear that the grayscale distribution reverts its gradient when changing the sign of the external field, according to a reversal of the microspin configuration and consequently to a reversal of the z-component of the magnetic induction field, which is sampled by MFM. As a preliminary observation, we comment that within the logic element evidenced by the dashed ellipse a double domain configuration is reached, featuring a Block domain wall aligned parallel to the minor axis; in the outer volume, considering the big extent (> 1 µm) of the smooth grey gradient belonging to the big "phantom" region above each element, we can conclude that it could be consistent with a magnetic induction region uniformly directed along the major axis. On the following section we will analyze in detail the field distribution introducing the differential approach.

6

Figure 3. a) AFM topographic image of six Co elements (sample C): major axis 1700±100 nm, minor axis 380±20 nm (aspect ratio 4.5:1), thickness 55±3 nm; white bar 1.7 µm. b) MFM registered magnetic contrast image of the same sample portion at H = -100 Oe; same scale as in a). c) MFM image of a single dot magnetic field distribution, subtracted by the SEM, at -100 Oe; black bar 250 nm. d) MFM image of a single dot magnetic field distribution, subtracted by the SEM, at +100 Oe; same scale as in d).

4. Discussion

4.1. Magnetostatic coupling

To evaluate the magnetostatic coupling, necessary to propagate the binary information along a MQCA chain, we performed a further differential analysis. The "switching" was computed by subtracting the "negative" frame from the "positive" one, in the two main states: at "high" external magnetic field, between H=+100 and H=-100 Oe, corresponding to the condition of *data write*, and at zero external magnetic field, between positive and negative remanence, corresponding to the condition *data retain*. The output is shown in Figure 4, where the differential magnetic information is represented according to an arbitrary color scale.

Figure 4. Enhanced differential MFM maps (color scale, arbitrary units) of a portion comprising 3 rows and 2 columns of elliptical elements, sample B (a, b) and C (c, d), computed at the *data write* state (a, c) and *data retain* (b, d).

Since the chromatic anisotropy reflects an out-of-plane magnetic field variation detected by the instrument tip, it is easy to read out that, by cycling the magnetic field between -100 and +100 Oe, the magnetization is inverted according to the external field orientation (Figure 4a, sample B), showing a regular distribution. No clear contrast may be found in the volume in between logic elements. For what concerns sample C in the *data write* state, inside the pillar a multi-domain state is developed: red/blue/red represent at least two regions generating a uniform out-of-plane magnetic field component. On the contrary, in between each element couple the equivalent of a single dipole state is achieved (blue/red), with an extension bigger than 1 µm. Thus the magnetic configuration at negative saturation is complementary to that found at positive saturation and is suitable

for the binary codification of information, realizing what we have called QSDL. This result is not obvious, since what we have realized is not a single domain nanomagnet chain, but rather a micrometric array which can be easily accessed by low magnetic fields (around 100 Oe) and could be read by fast magneto-optical devices, since the affected zone also includes the inter-element volume.

The ultimate data retention test has to be done at remanence, where zero external field, equivalent to no stimuli, should give a bistable output, depending on the magnetic history of the element chain. The result is presented again in Figure 4: sample B (panel b) is characterized by a weaker data retention capability, since the contrast is low and it is difficult to describe the structures, mainly pinned on each element rim. On the contrary, in sample C (panel d) the single element is split into two magnetic domains, probably separated by a vertical Bloch wall (violet region in the middle of the pillar) which is able to store information. Also the rim of each element is such that useful information is stored in it. A faint magnetic induction distribution is visible in between the elements.

Based on these considerations, we prepared a graphic map relative to a possible local spin arrangement within the samples. Figure 5 is equivalent to Figure 4a; the magnetization distribution, as well as the magnetic induction field, may be conveniently substituted by visualizing the equivalent concatenated current (black arrows), evidencing the inter-element interaction paths. Figure 6 is equivalent to Figure 4c; here the stronger collective behavior results in a meandering path of the equivalent concatenated current, in between chains of logic elements.

Figure 5. Local spin arrangement for sample B in the *data write* state, superimposed on the differential MFM map. The white arrows represent the magnetization within each element, their heads being equivalent to their tails. The colored lines represent magnetic induction, when continuous above the film plane, when dashed below the film plane. The black arrows represent the equivalent induced current concatenated with the flux distribution.

Figure 6. Local spin arrangement for sample C in the *data write* state: hypothesis relative to the local spin arrangement and equivalent concatenated current distribution.

4.2. FEM simulation

Since the z-component of the induction field developed in a patterned array is responsible for the MFM signal evidenced in Figure 4, we performed FEM simulations of an arbitrarily magnetized array of 9 Co elements over bulk Si having the same geometry of the real sample in order to qualitatively reproduce the field distribution (Figure 7). In particular the tapered profile typical of lift-off was reproduced in the model geometry. The use of a commercial FEM code (Comsol Multiphysics®) based on magnetostatics is necessary, given the enormous number of elements arising from both a big control volume (80 μm^3) and a small tetrahedral Lagrangian cubic element mesh in correspondence of the magnetic discs (around 0.01 μm^3). The complexity of the system is very high, having 150k elements, with a number of degrees of freedom of about 170k and a solution time (Intel® Core[TM] 2 Quad Q9550 2.83 GHz, 4 GB DDR3) around 220 s.

Based on the MFM maps obtained at remanence, we propose the microspin arrangement indicated in Figure 7b, where four uniform regions may be evidenced: the outer edge and the zone around the minor axis, magnetized perpendicularly with respect to the film plane, and the two portions magnetized with a small skew angle with respect to the easy, major axis of the ellipse.

Figure 7. a) FEM control volume showing the Si substrate (green) and the Co logic elements (blue). b) microspin arrangement in the proposed remanence configuration for an elliptical tapered Co element.

The field distribution of this system is represented in Figure 8, where both the strength of the azimuthal component (Bz) of the magnetic flux density and the angle of the radial one (atan(By/Bx)) were evaluated, along [x-y] planes parallel to the Si substrate face at various heights: 0 nm (panels a and d), 100 nm (panels b and e) and 500 nm (panels c and f). In particular the position of the MFM tip during a typical scan is 100 nm above the sample, equivalent to the 100-nm-plane simulated in Figures 8b and 8e. Figure 8b, which represents a static configuration, is to be compared with Figure 4, which in turn represents a differential configuration but featuring a qualitatively similar azimuthal distribution.

Figure 8. Distribution of the azimuthal component of the magnetic flux density in correspondence of [x-y] planes at various heights with respect to the Si substrate: 0 nm (a), 100 nm (b) and 500 nm (c). Distribution of the direction of the radial component of the magnetic flux density in correspondence of [x-y] planes at various heights with respect to the Si substrate: 0 nm (d), 100 nm (e) and 500 nm (f).

5. Conclusions

This study highlights the engineering of a MQCA configuration. We proposed and realized a MQCA based on elliptical elements featuring micrometric spacing and micrometric major axis, realized by means of cost-effective techniques such as RF sputtering and lift-off, that switch applying an external magnetic field in the plane of the film. Enhanced MFM images were used to compute the differential map between positive and negative states, both at saturation (*data write*) and remanence (*data retain*), actually demonstrating the occurrence of the switching and the presence of a bi-stable magnetostatic inter-element dipolar coupling, resulting in a configuration similar to the single domain state of a nanometric magnet. FEM simulations helped to validate the experimentally measured azimuthal field distributions. Currently, our experiments are performed towards the implementation of the "snake-clock" architecture, proposed in a previous work [15].

[1]   C. S. Lent, P. D.Tougaw, W. Porod and G. H. Bernstein, Quantum cellular automata, *Nanotechnology*, **1993**, 4, 49;

[2]   A. I. Csurgay, W. Porod, and C. S. Lent, Signal processing with near-neighbor coupled time-varying quantum-dot arrays, *IEEE Trans. On Circuits and Systems*, **2000**, I47, 1212;

[3]   A. O. Orlov, I. Amlani, G. H. Bernstein, C. S. Lent, and G. L. Snider, Realization of a functional cell for Quantum-dot Cellular Automata, *Science*, **1997** 277, 928;

[4]   I. Amlani, A. O. Orlov, G. Toth, G. H. Bernstein, C. S. Lent, and G. L. Snider, Digital logic gate using Quantum-dot Cellular Automata, *Science*, **1999**, 284, 289;

10

[5]   K. Kummamuru, A. O. Orlov, R. Ramasubramaniam, C.S. Lent, G. H.Bernstein, and G. L. Snider, Operation of a Quantum-dot Cellular Automata (QCA) shift register and analysis of errors, *IEEE Trans. on Electron Devices*, **2003**, 50,1906;

[6]   Alexandra Imre, "Experimental study of nanomagnets for Quantum-dot cellular automata (MQCA) logic applications", PhD thesis;

[7]   L. Ouattara, M. Knutzen, S. Keller, M.F. Hansen, A. Boisen, Double layer resist process scheme for metal lift-off with application in inductive heating of microstructures, *Microelectronic Engineering*, **2000**, 87, 1226–1228;

[8]   P. Tiberto, S. Gupta, S. Bianco, F. Celegato, P. Martino, A. Chiolerio, A. Tagliaferro and P. Allia, Morphology and magnetic properties of island-like Co and Ni films obtained by de-wetting, *J. Nanoparticle Research*, **2010**, DOI 10.1007./s11051-010-0023-2;

[9]   A. Chiolerio, E. Celasco, F. Celegato, S. Guastella, P. Martino, P. Allia, P. Tiberto and F. Pirri, Enhanced imaging of magnetic structures in micropatterned arrays of Co dots and antidots, *J. of Magnetism and Magnetic Materials*, **2008**, 320, 669 – 673;

[10]   A. Chiolerio, P. Allia, A. Chiodoni, F. Pirri, F. Celegato and M. Coisson, Thermally evaporated Cu-Co top spin valve with random exchange bias, *J. Appl. Phys.,* **2007**, 101, 123915;

[11]   A. Chiolerio, P. Allia, P. Tiberto and M. Coisson, Magnetic and magnetotransport properties of a Co-Sn evaporated trilayer, *J. Phys.: Cond. Matt.*, **2008**, 20, 345213;

[12]   R. P. Cowburn, A. O. Adeyeye and M. E. Welland, Controlling magnetic ordering in coupled nanomagnet arrays, *New Journal of Physics*, **1999**, 1 161;

[13]   G.H. Bernstein, A. Imre, V. Metlushko, A. Orlov, L. Zhou, L. Ji, G. Csaba, W. Porod, Magnetic QCA systems, *Microelectronics Journal*, **2005**, 36, 619-624;

[14]   A. Chiolerio, P. Martino, F. Celegato, S. Giurdanella and P. Allia, Enhancement and correlation of MFM images: effect of the tip on the magnetic configuration of patterned Co films, *IEEE Trans. Mag.*, **2010**, 46, 195-198;

[15]   M. Graziano, M. Vacca, A. Chiolerio and M. Zamboni, A NCL-HDL snake-clock logic for Magnetic Quantum Cellular Automata, *IEEE Transactions on Nanotechnology*, **2011**, 10, 1141-1149.
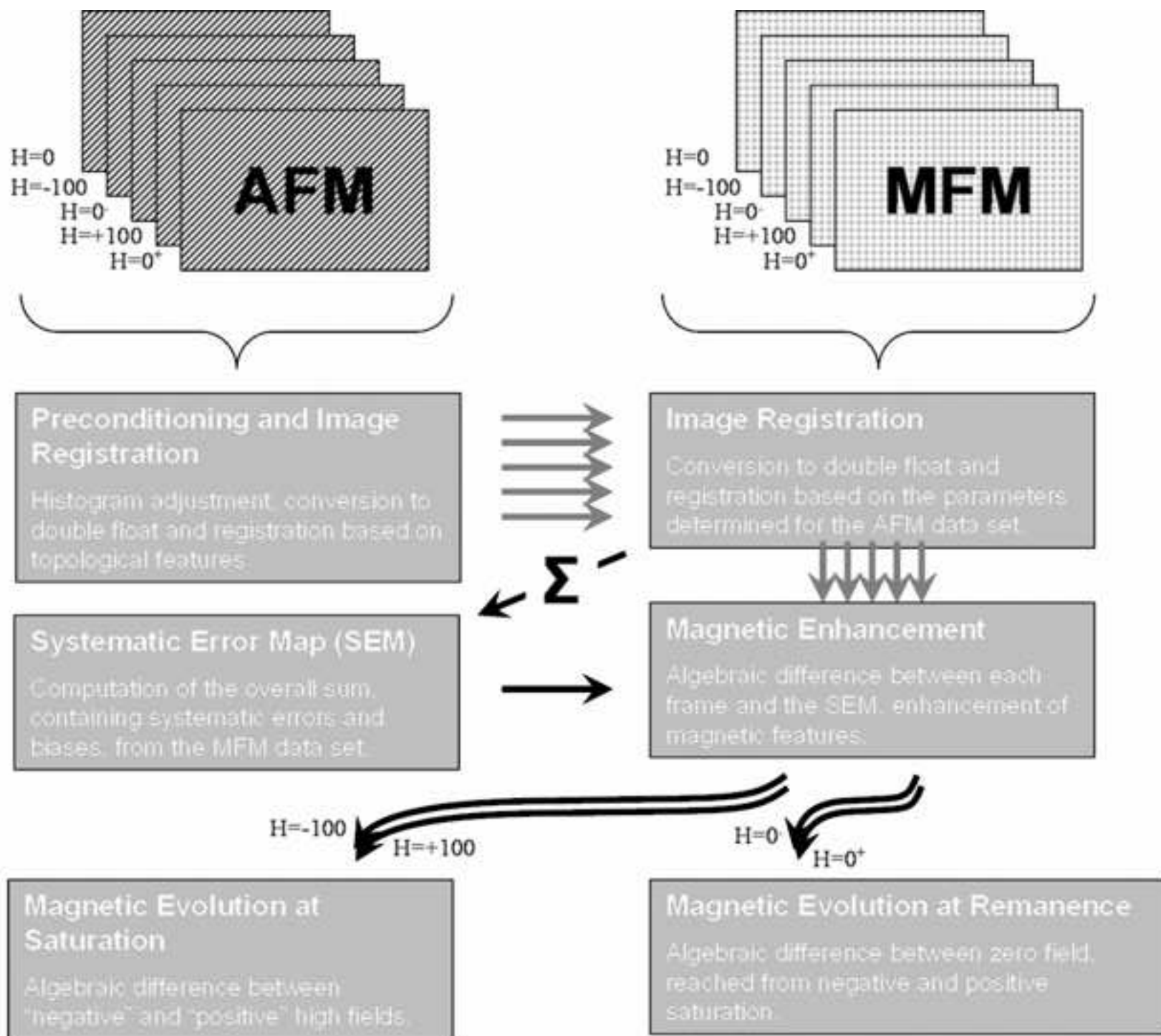
Figure 1
Click here to download high resolution image

Figure 2
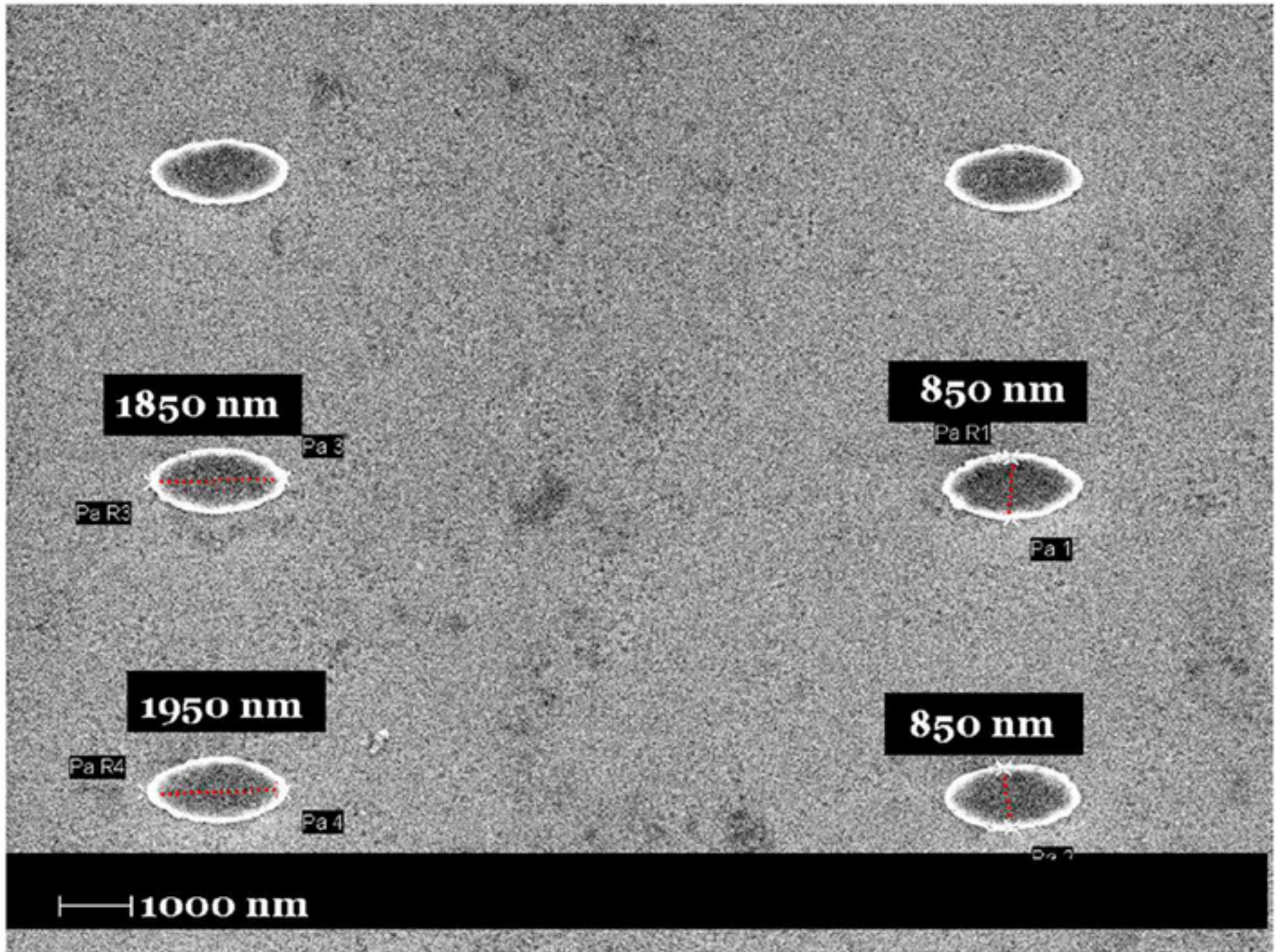**Click here to download high resolution image**

Figure 3
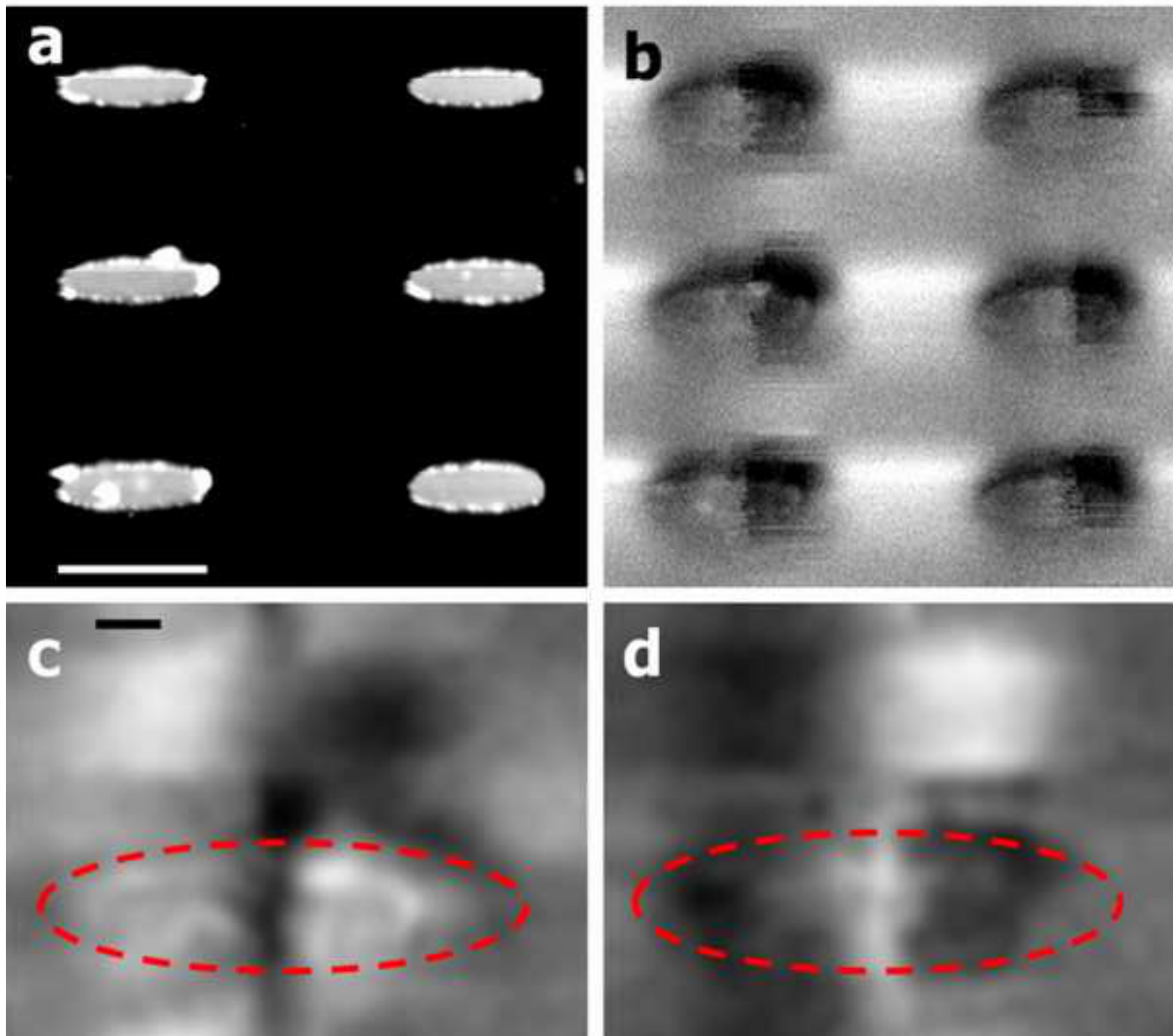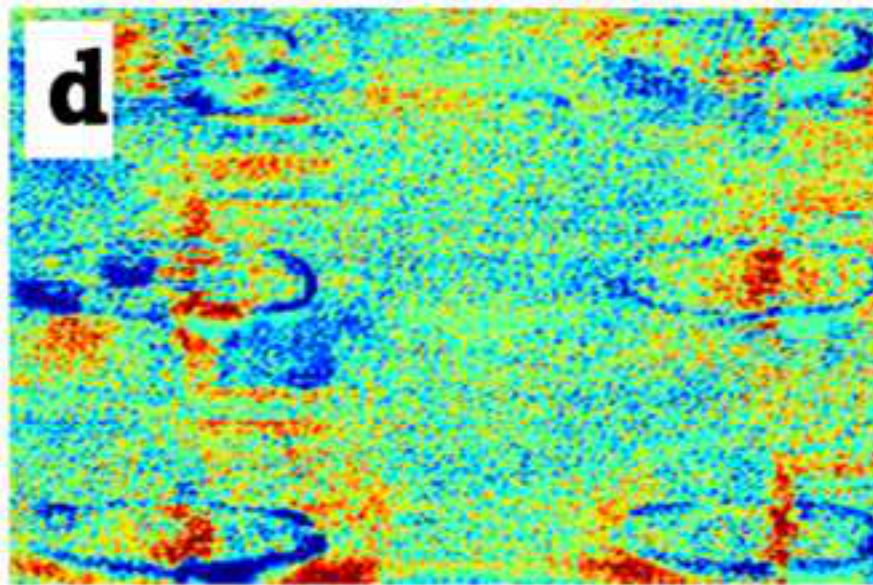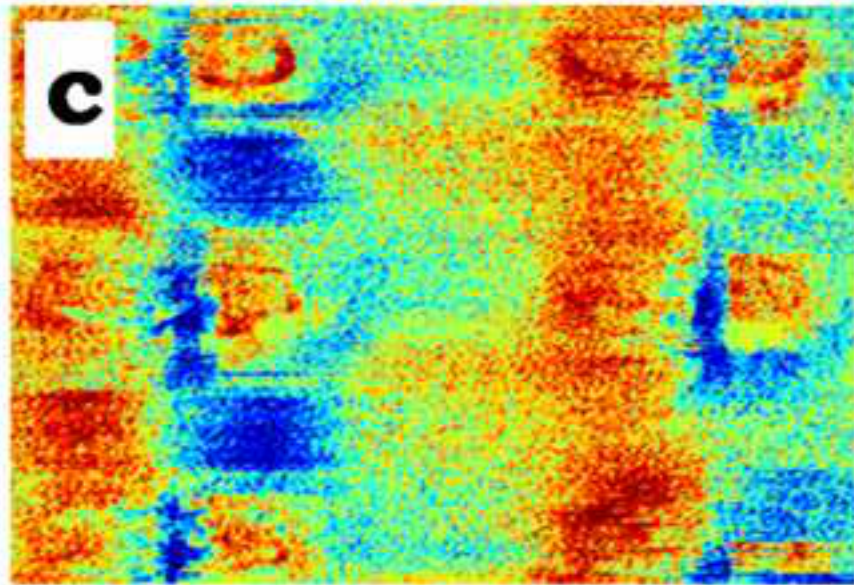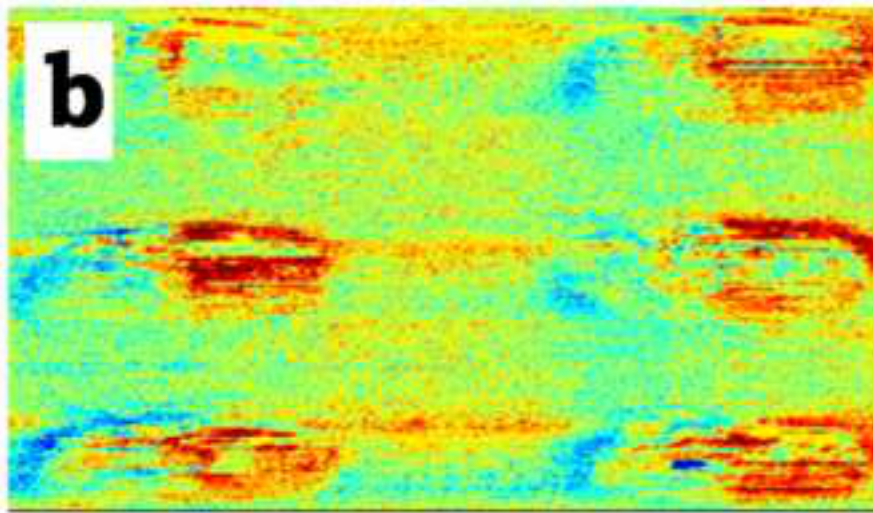**Click here to download high resolution image**
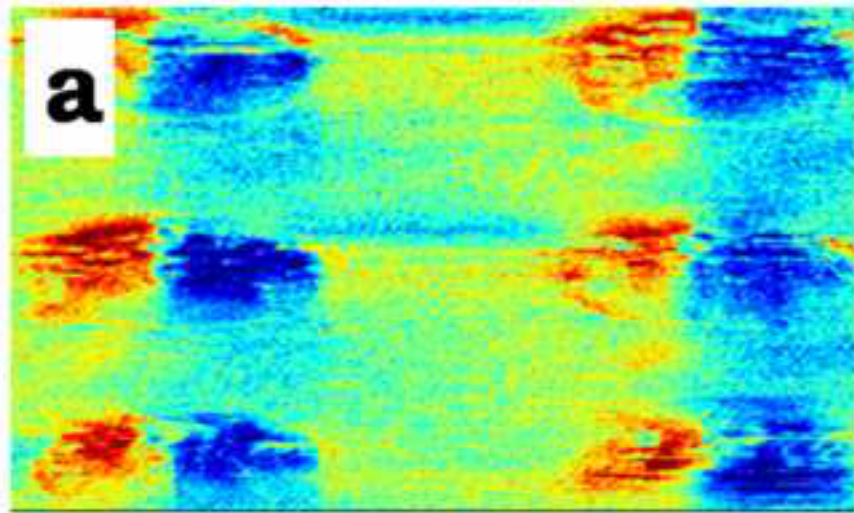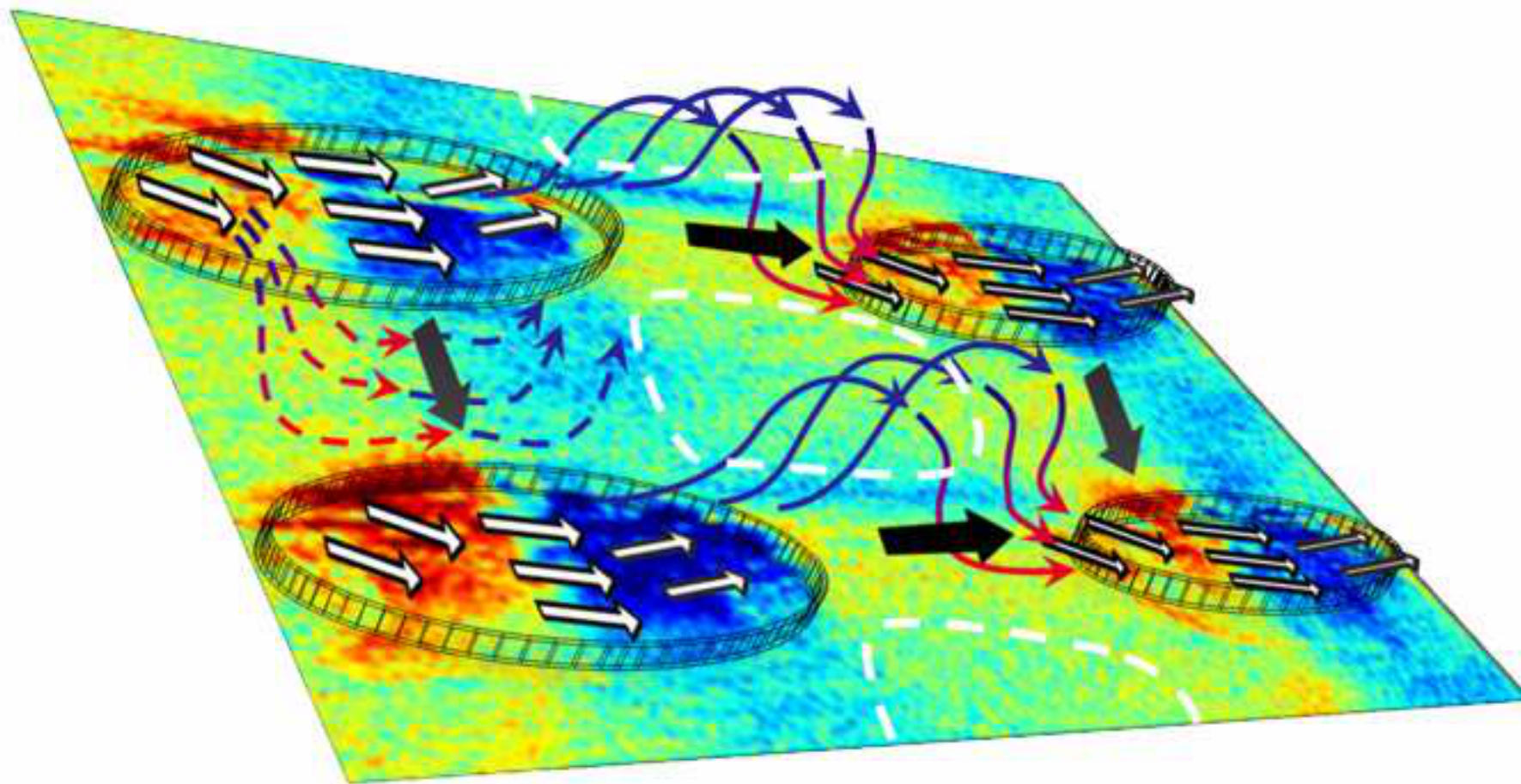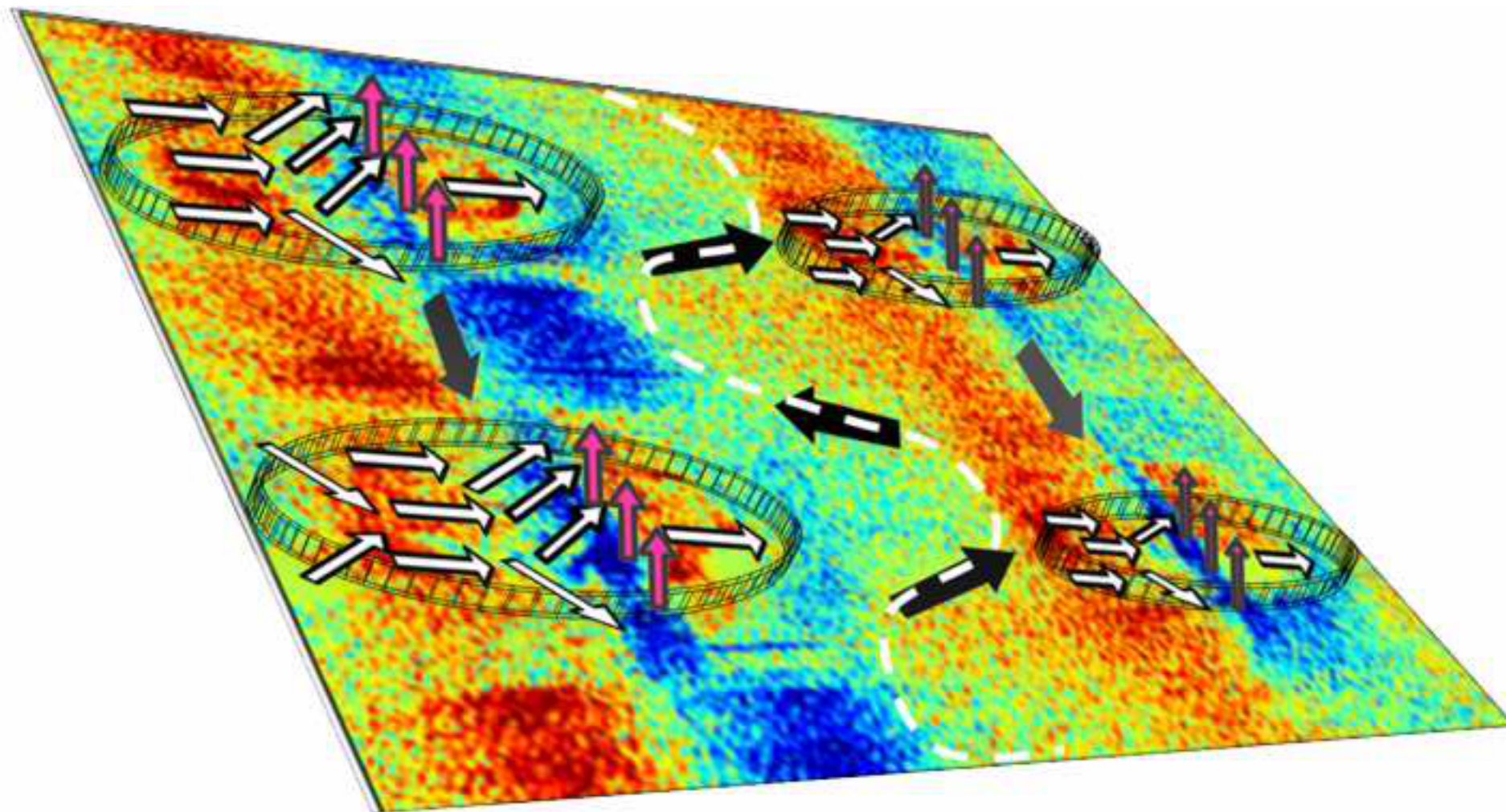
Figure 4
Click here to download high resolution image

Figure 5
Click here to download high resolution image

Figure 6
Click here to download high resolution image

Figure 7
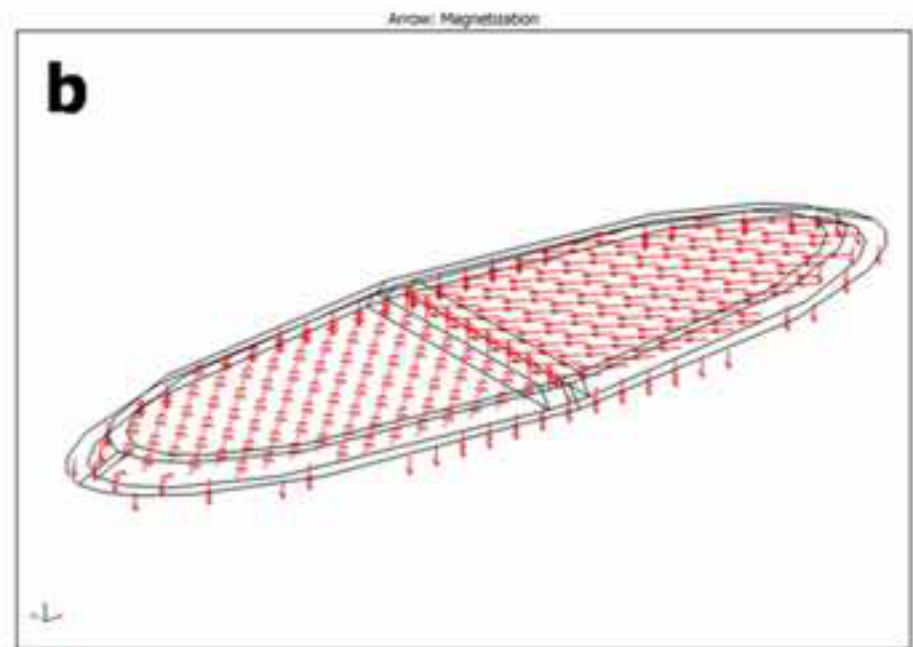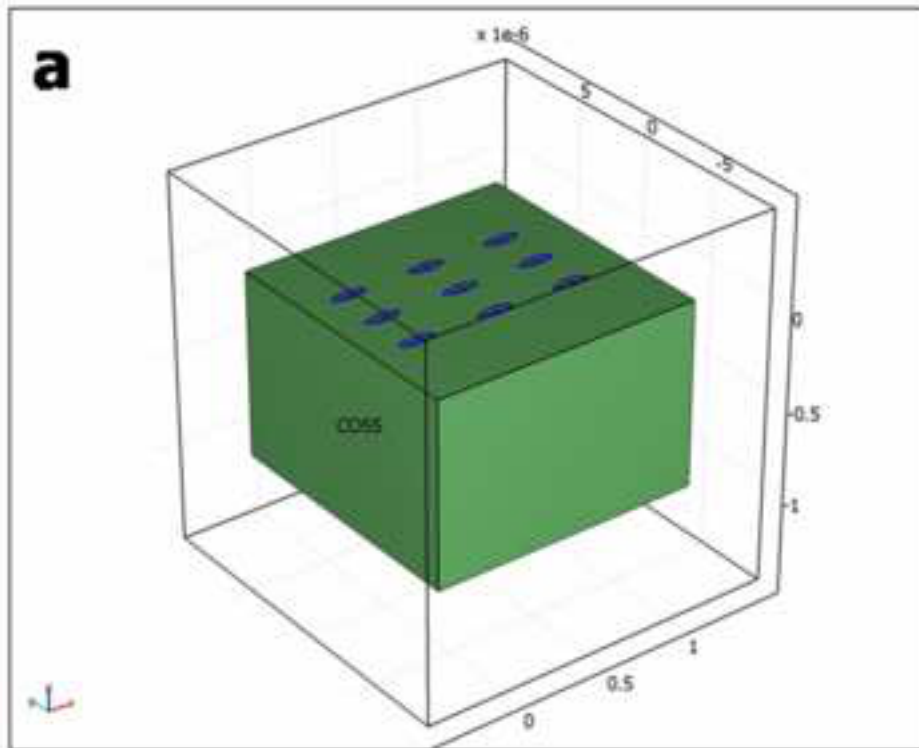**Click here to download high resolution image**

Figure 8
Click here to download high resolution image